

Unitary Fermi gas at finite temperature in the ϵ expansion

Yusuke Nishida*

Department of Physics, University of Tokyo, Tokyo 113-0033, Japan and
Institute for Nuclear Theory, University of Washington, Seattle, Washington 98195-1550, USA

(Dated: August 2006)

Thermodynamics of the unitary Fermi gas at finite temperature is investigated from the perspective of the expansion over $\epsilon = 4 - d$ with d being the dimensionality of space. We show that the thermodynamics is dominated by bosonic excitations in the low temperature region where $T \ll T_c$. Analytic formulas for the thermodynamic functions as functions of the temperature are derived to the lowest order in ϵ in this region. In the high temperature region where $T \sim T_c$, bosonic and fermionic quasiparticles are excited and we determine the critical temperature T_c and the thermodynamic functions around T_c to the leading and next-to-leading orders in ϵ .

PACS numbers: 05.30.Fk, 03.75.Ss, 05.70.Ce

I. INTRODUCTION

The Fermi gas with zero-range interaction at infinite scattering length [1, 2, 3], frequently referred to as the unitary Fermi gas, has attracted intense attention across many subfields of physics. Experimentally, the system can be realized in atomic traps using the Feshbach resonance and has been extensively studied [4, 5, 6, 7, 8, 9, 10]. Since the fermion density is the only dimensionful scale of the unitary Fermi gas, its properties are universal, i.e., independent of details of the interparticle interaction. The unitary Fermi gas is an idealization of dilute nuclear matter and may be relevant for the physics of neutron stars [11]. It has been also suggested that its understanding may be important for the high- T_c superconductivity [12].

The austere simplicity of the unitary Fermi gas implies great difficulties for theoretical treatments, because there seems to be no parameter for a perturbation theory. Recently, we have proposed a new approach for the unitary Fermi gas based on the systematic expansion in terms of the dimensionality of space [13, 14], utilizing the specialty of *four* or *two* spacial dimensions in the unitarity limit [15]. In this approach, one would extend the problem to arbitrary spatial dimensions d and consider d is close to four or two. Then one performs all calculations treating $\epsilon = 4 - d$ or $\bar{\epsilon} = d - 2$ as a small parameter of the perturbative expansion. Results for the physical case of three spatial dimensions are obtained by extrapolating the series expansions to $\epsilon(\bar{\epsilon}) = 1$, or more appropriately, by matching two series expansions.

We used this ϵ expansion around four spatial dimensions to calculate thermodynamic quantities and fermion quasiparticle spectrum in the unitarity limit and found results which are quite consistent with those obtained by Monte Carlo simulations and experiments [13, 14]. This ϵ expansion has been successfully applied to atom-dimer and dimer-dimer scatterings in vacuum [16]. Thus there

are compelling reasons to hope that the limit $d \rightarrow 4$ is not only theoretically interesting but also practically useful, despite the fact that the expansion parameter ϵ is one. Very recently, the phase structure of polarized Fermi gas has been investigated based on the ϵ expansion [14, 17].

In this paper, we extend our approach to investigate the thermodynamics of unitary Fermi gas at finite temperature T , below and above the critical temperature $T = T_c$. So far, such a problem has been studied relying on the mean-field description with fluctuations [18, 19, 20, 21, 22, 23, 24, 25, 26, 27], the virial expansion [28, 29, 30], or the Monte Carlo simulations [31, 32, 33, 34, 35]. The main advantage of our approach is that $\epsilon = 4 - d$ provides the small parameter of the perturbative expansion, and thus, analytic and systematic study below and above T_c is possible. We also note that the critical dimension of a superfluid-normal phase transition is also four, which makes weak-coupling calculations reliable at any temperature for the small ϵ .

First, we review the ϵ expansion for the unitary Fermi gas around four spatial dimensions in Sec. II. Then we discuss that the thermodynamics in the low temperature region $T \ll T_c$ is dominated by bosonic excitations. Analytic formulas for the thermodynamic functions as functions of the temperature to the lowest order in ϵ is shown in Sec. III. The behavior of the thermodynamic functions above T_c to the leading and next-to-leading orders in ϵ is discussed in Sec. IV. In particular, we put emphasis on the determination of the critical temperature T_c by matching the ϵ expansion with the expansion around two spatial dimensions. The thermodynamic functions at T_c are also calculated, which are compared to the results from recent Monte Carlo simulations. Finally, summary and concluding remarks are given in Sec. V.

*Electronic address: nishida@nt.phys.s.u-tokyo.ac.jp

II. REVIEW OF ϵ EXPANSION

Here we briefly review the ϵ expansion for the unitary Fermi gas around four spatial dimensions and quote some results at zero temperature to the leading order in ϵ just for the convenience of later discussions at finite temperature. The detailed account of the ϵ expansion is found in Refs. [13, 14].

A. Lagrangian and Feynman rules

The extension to the finite temperature T follows from the prescription of the imaginary time formalism. The system under consideration is described by the following Lagrangian density with a local four-Fermi interaction (here and below $\hbar = 1$):

$$\mathcal{L}_0 = \Psi^\dagger \left(\partial_\tau - \frac{\sigma_3 \nabla^2}{2m} - \sigma_+ \phi_0 - \sigma_- \phi_0 \right) \Psi + \varphi^* \left(\partial_\tau - \frac{\nabla^2}{4m} \right) \varphi + \frac{\phi_0^2}{c_0}, \quad (1)$$

$$\mathcal{L}_1 = -g \Psi^\dagger \sigma_+ \Psi \varphi - g \Psi^\dagger \sigma_- \Psi \varphi^* - \mu \Psi^\dagger \sigma_3 \Psi - \left(2\mu - \frac{g^2}{c_0} \right) \varphi^* \varphi + \frac{g\phi_0}{c_0} \varphi + \frac{g\phi_0}{c_0} \varphi^*, \quad (2)$$

$$\mathcal{L}_2 = -\varphi^* \left(\partial_\tau - \frac{\nabla^2}{4m} \right) \varphi + 2\mu \varphi^* \varphi. \quad (3)$$

The propagators of fermion and boson are generated by \mathcal{L}_0 . The fermion propagator is a 2×2 matrix,

$$G(i\omega_n, \mathbf{p}) = \frac{1}{(i\omega_n)^2 - E_{\mathbf{p}}^2} \begin{pmatrix} i\omega_n + \varepsilon_{\mathbf{p}} & -\phi_0 \\ -\phi_0 & i\omega_n - \varepsilon_{\mathbf{p}} \end{pmatrix}, \quad (4)$$

where $\varepsilon_{\mathbf{p}} = \mathbf{p}^2/2m$ is the kinetic energy of non-relativistic particles and ϕ_0 is the condensate in the superfluid ground state. $E_{\mathbf{p}} = \sqrt{\varepsilon_{\mathbf{p}}^2 + \phi_0^2}$ is the excitation energy of the fermion quasiparticle. The boson propagator D is

$$D(i\nu_n, \mathbf{p}) = \left(i\nu_n - \frac{\varepsilon_{\mathbf{p}}}{2} \right)^{-1}. \quad (5)$$

$\omega_n = 2\pi T(n + \frac{1}{2})$ and $\nu_n = 2\pi Tn$ are discrete Matsubara frequencies for fermion and boson with an integer $n = 0, \pm 1, \pm 2, \dots$. The unitary Fermi gas around four spatial dimensions is described by the weakly-interacting system of fermionic and bosonic quasiparticles, whose coupling $g \sim \epsilon^{1/2}$ in \mathcal{L}_1 is given by

$$g = \frac{(8\pi^2 \epsilon)^{1/2}}{m} \left(\frac{m\phi_0}{2\pi} \right)^{\epsilon/4}. \quad (6)$$

We define the counter vertex in \mathcal{L}_2 for the boson propagator as

$$\Pi_0(p_0, \mathbf{p}) = p_0 - \frac{\varepsilon_{\mathbf{p}}}{2}, \quad (7)$$

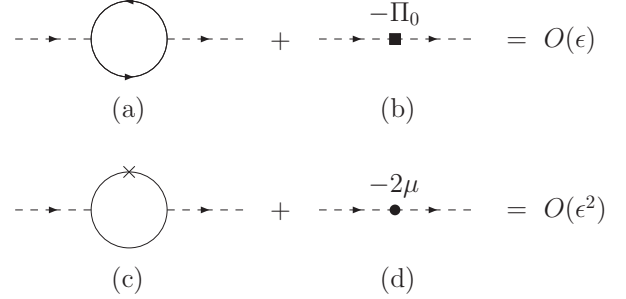


FIG. 1: Restoration of naive ϵ counting for the boson self-energy. The fermion loop in (c) goes around clockwise and counterclockwise. Solid (dotted) lines represent the fermion (boson) propagator $-G$ ($-D$), while the cross in (c) represents the μ insertion to the fermion propagator.

and the boson chemical potential as

$$\mu_B = 2\mu - \frac{g^2}{c_0}. \quad (8)$$

When c_0 is negative, $-g^2/c_0 \simeq \varepsilon_b$ gives the binding energy of boson to the leading order in ϵ . Throughout this paper, we consider the vicinity of the unitary point where $\varepsilon_b \sim \epsilon \phi_0$.

B. Power counting rule of ϵ

The power counting rule of ϵ is summarized as follow:

1. We consider $\mu/\phi_0 \sim \epsilon$ and regard ϕ_0 as $O(1)$.
2. For any Green's function, we write down all Feynman diagrams according to the Feynman rules using the propagators from \mathcal{L}_0 and the vertices from \mathcal{L}_1 .
3. If there is any subdiagram of the type in Fig. 1(a) or Fig. 1(c), we add a diagram where the subdiagram is replaced by a vertex from \mathcal{L}_2 , Fig. 1(b) or Fig. 1(d).
4. The power of ϵ for the given Feynman diagram will be $O(\epsilon^{N_g/2 + N_\mu})$, where N_g is the number of couplings g and N_μ is the number of chemical potential insertions.
5. The only exception is the one-loop vacuum diagram of fermion with one μ insertion, which is $O(1)$ instead of the naive $O(\epsilon)$.

This power counting rule holds in the low temperature region where the condensate is still large compared to the chemical potential $\mu/\phi_0 \sim \epsilon$, while it breaks down near the critical temperature because $\phi_0 \rightarrow 0$ at $T \rightarrow T_c$. In the high temperature region $T \sim T_c$, a minor modification of the power counting rule is necessary as we discuss in Sec. IV.

C. Leading order results at $T = 0$

Here we show only leading order results on the thermodynamic functions at zero temperature, which is equivalent to the mean-field approximation. The results to the next-to-leading order in ϵ are found in Refs. [13, 14]. The effective potential to the leading order in ϵ is

$$V_{\text{eff}}(\phi_0) = \left[\frac{\phi_0}{3} - \frac{\mu_B}{2\epsilon} \right] \left(\frac{m\phi_0}{2\pi} \right)^{d/2}, \quad (9)$$

from which the condensate follows as

$$\phi_0 = \frac{\mu_B}{\epsilon}. \quad (10)$$

Note that the previously made assumption $\mu/\phi_0 = O(\epsilon)$ is now checked. Then the pressure at zero temperature is given by

$$P_0 = -V_{\text{eff}}(\phi_0) = \frac{\phi_0}{6} \left(\frac{m\phi_0}{2\pi} \right)^{d/2}. \quad (11)$$

From the fermion number density

$$N = \frac{\partial P_0}{\partial \mu} = \frac{1}{\epsilon} \left(\frac{m\phi_0}{2\pi} \right)^{d/2}, \quad (12)$$

we define the Fermi energy through the relationship in the ideal Fermi gas at d spatial dimensions;

$$\varepsilon_F = \frac{2\pi}{m} \left[\frac{1}{2} \Gamma \left(\frac{d}{2} + 1 \right) N \right]^{2/d} = \frac{\phi_0}{\epsilon^{2/d}}. \quad (13)$$

The energy density is given by

$$E_0 = \mu N - P_0 = \left[\frac{\phi_0}{3} - \frac{\varepsilon_b}{2\epsilon} \right] \left(\frac{m\phi_0}{2\pi} \right)^{d/2}, \quad (14)$$

where $\varepsilon_b = -g^2/c_0 > 0$ is the binding energy of boson. The chemical potential at the fixed Fermi energy ε_F is obtained from Eqs. (10) and (13) as

$$\mu_0 = \frac{\epsilon^{3/2}}{2} \varepsilon_F - \frac{\varepsilon_b}{2}. \quad (15)$$

III. THERMODYNAMICS BELOW T_c

Now we investigate the thermodynamics of the Fermi gas at finite temperature near the unitarity limit. At zero temperature, we found that there exist two difference energy scales in the system; the scale of condensate ϕ_0 and that of chemical potential $\mu \sim \epsilon\phi_0 \ll \phi_0$. Accordingly, we can consider two temperature regions where the unitary Fermi gas exhibits different thermodynamics.

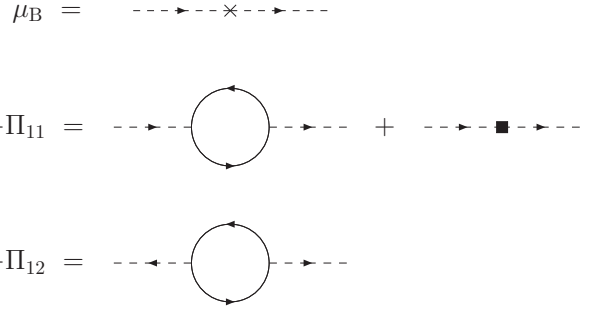


FIG. 2: Boson's self-energies contributing to the order $O(\epsilon)$. The vertex Π_0 from \mathcal{L}_2 needs to be added to the second diagram. The last diagram gives the off-diagonal part of the self-energy.

One is the low temperature region where $T \sim \epsilon\phi_0$. In this region, the energy gap of the fermion quasiparticle $\Delta \sim \phi_0$ is still large compared to the temperature. Therefore, thermal excitations of the fermion quasiparticle are exponentially suppressed by a factor $e^{-\Delta/T} \sim e^{-1/\epsilon}$. The thermodynamics in this region is dominated by the bosonic phonon excitations. The other temperature region is the high temperature region where $T \sim \phi_0$. (ϕ_0 represents the condensate at zero temperature.) In this region, the condensate decreases and eventually vanishes at the critical temperature T_c . Fermions and bosons are equally excited here. We defer our discussion on the high temperature region to Sec. IV and concentrate on the thermodynamics at the low temperature region $T \ll T_c$ in this section.

A. Phonon spectrum

The thermodynamics at the low temperature region $T \ll \phi_0$ is dominated by the phonon excitations. In order to determine the phonon spectrum, we first study the boson self-energy at zero temperature. To the order of $O(\epsilon)$, there are three types of contributions to the boson self-energy as depicted in Fig. 2. In addition to the chemical potential insertion $\mu_B = 2\mu + \varepsilon_b$, the one-loop diagrams contribute to the diagonal part Π_{11} and off-diagonal part Π_{12} of the boson self-energy. The vertex Π_0 from \mathcal{L}_2 is necessary for Π_{11} according to the power counting rule described in Sec. II. Then the diagonal part of the boson self-energy is given by

$$\Pi_{11}(p) = \Pi_0(p) + \Pi_a(p), \quad (16)$$

where Π_0 is defined in Eq. (7) and Π_a is given by

$$\begin{aligned}
-\Pi_a(p) &= g^2 \int \frac{i dk_0 dk}{(2\pi)^{d+1}} G_{11}\left(k + \frac{p}{2}\right) G_{22}\left(k - \frac{p}{2}\right) \\
&= g^2 \int \frac{d\mathbf{k}}{(2\pi)^d} \frac{1}{4E_{\mathbf{k}-\frac{p}{2}} E_{\mathbf{k}+\frac{p}{2}}} \left[\frac{(E_{\mathbf{k}-\frac{p}{2}} + \varepsilon_{\mathbf{k}-\frac{p}{2}})(E_{\mathbf{k}+\frac{p}{2}} + \varepsilon_{\mathbf{k}+\frac{p}{2}})}{E_{\mathbf{k}-\frac{p}{2}} + E_{\mathbf{k}+\frac{p}{2}} - p_0} + \frac{(E_{\mathbf{k}-\frac{p}{2}} - \varepsilon_{\mathbf{k}-\frac{p}{2}})(E_{\mathbf{k}+\frac{p}{2}} - \varepsilon_{\mathbf{k}+\frac{p}{2}})}{E_{\mathbf{k}-\frac{p}{2}} + E_{\mathbf{k}+\frac{p}{2}} + p_0} \right]. \tag{17}
\end{aligned}$$

Since we are interested in physics at the scale of temperature $T \ll \phi_0$, it is sufficient to evaluate the self-energy when the external momentum is small $p \sim T \ll \phi_0$. Expanding $\Pi_{11}(p)$ in terms of p/ϕ_0 and performing the \mathbf{k} integration with the use of the formula

$$\int_0^\infty dz \frac{z^{\alpha-1}}{(z+1)^\beta} = \frac{\Gamma(\alpha)\Gamma(\beta-\alpha)}{\Gamma(\beta)}, \tag{18}$$

we obtain

$$\Pi_{11}(p) \simeq -g^2 \int \frac{d\mathbf{k}}{(2\pi)^d} \frac{E_{\mathbf{k}}^2 + \varepsilon_{\mathbf{k}}^2}{4E_{\mathbf{k}}^3} = \frac{3}{2}\epsilon\phi_0 + O(\epsilon^2). \tag{19}$$

Similarly, the off-diagonal part of the boson-self energy is given by

$$\begin{aligned}
-\Pi_{12}(p) &= g^2 \int \frac{i dk_0 dk}{(2\pi)^{d+1}} G_{12}\left(k + \frac{p}{2}\right) G_{12}\left(k - \frac{p}{2}\right) \\
&= -g^2 \int \frac{d\mathbf{k}}{(2\pi)^d} \frac{\phi_0^2}{4E_{\mathbf{k}-\frac{p}{2}} E_{\mathbf{k}+\frac{p}{2}}} \times \\
&\quad \left[\frac{1}{E_{\mathbf{k}-\frac{p}{2}} + E_{\mathbf{k}+\frac{p}{2}} - p_0} + \frac{1}{E_{\mathbf{k}-\frac{p}{2}} + E_{\mathbf{k}+\frac{p}{2}} + p_0} \right]. \tag{20}
\end{aligned}$$

Expanding $\Pi_{12}(p)$ in terms of p/ϕ_0 and performing the integration over \mathbf{k} , we obtain

$$\Pi_{12}(p) \simeq g^2 \int \frac{d\mathbf{k}}{(2\pi)^d} \frac{\phi^2}{4E_{\mathbf{k}}^3} = \frac{1}{2}\epsilon\phi_0 + O(\epsilon^2). \tag{21}$$

As a result of the resummation of these self-energies, the resummed boson propagator \tilde{D} is expressed by the following 2×2 matrix:

$$\begin{aligned}
\tilde{D}(p_0, \mathbf{p}) &= \\
\begin{pmatrix} D(p)^{-1} + \mu_B - \Pi_{11} & -\Pi_{12} \\ -\Pi_{21} & D(-p)^{-1} + \mu_B - \Pi_{22} \end{pmatrix}^{-1}, \tag{22}
\end{aligned}$$

where $\Pi_{22} = \Pi_{11}$ and $\Pi_{12} = \Pi_{21}$. The dispersion relation of the boson $\omega_{\text{ph}}(\mathbf{p})$ can be obtained by solving the equation $\det[D^{-1}(\omega, \mathbf{p})] = 0$ in terms of ω as

$$\omega_{\text{ph}}(\mathbf{p}) = \sqrt{\left(\frac{\varepsilon_{\mathbf{p}}}{2} - \mu_B + \epsilon\phi_0\right) \left(\frac{\varepsilon_{\mathbf{p}}}{2} - \mu_B + 2\epsilon\phi_0\right)}. \tag{23}$$

Note that this expression is valid as long as $\varepsilon_{\mathbf{p}} \ll \phi_0$ because of the expansions made to evaluate the boson self-energies. Substituting the solution of the gap equation

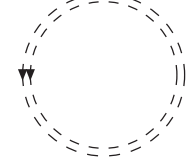


FIG. 3: One-loop diagram of boson contributing the effective potential at finite temperature. The dotted double line represents the resummed boson propagator \tilde{D} in Eq. (22).

at zero temperature in Eq. (10), $\mu_B = \epsilon\phi_0$, the phonon spectrum is determined to be

$$\omega_{\text{ph}}(\mathbf{p}) = \sqrt{\frac{\varepsilon_{\mathbf{p}}}{2} \left(\frac{\varepsilon_{\mathbf{p}}}{2} + \epsilon\phi_0 \right)}. \tag{24}$$

For the small momentum $\varepsilon_{\mathbf{p}} \ll \epsilon\phi_0$, the dispersion relation becomes linear in the momentum as $\omega_{\text{ph}} \simeq c_s |\mathbf{p}|$, remaining gapless in accordance with the Nambu-Goldstone theorem. The sound velocity of phonon c_s is given by

$$c_s = \sqrt{\frac{\epsilon\phi_0}{4m}} \sim \epsilon^{1/2}. \tag{25}$$

For the large momentum $\varepsilon_{\mathbf{p}} \gg \epsilon\phi_0$, the dispersion relation approaches that of the free boson as $\omega_{\text{ph}} \simeq \varepsilon_{\mathbf{p}}/2$.

B. Effective potential and condensate

At finite temperature, the phonon excitations contribute to the effective potential, and consequently, the magnitude of the condensate decreases. The temperature dependent part of the effective potential $V_T(\phi_0)$ to the lowest order in ϵ is given by the one-loop diagram of the boson with the resummed propagator in Eq. (22) [Fig. 3]:

$$\begin{aligned}
V_T(\phi_0) &= \frac{T}{2} \sum_n \int \frac{d\mathbf{p}}{(2\pi)^4} \text{Tr} \ln \left[\tilde{D}(i\nu_n, \mathbf{p})^{-1} \right] \\
&= \int \frac{d\mathbf{p}}{(2\pi)^4} T \ln \left[1 - e^{-\omega_{\text{ph}}(\mathbf{p})/T} \right]. \tag{26}
\end{aligned}$$

Then its contribution to the gap equation is

$$\frac{\partial V_T(\phi_0)}{\partial \phi_0} = \int \frac{d\mathbf{p}}{(2\pi)^4} f_B(\omega_{\text{ph}}) \frac{\partial \omega_{\text{ph}}}{\partial \phi_0}, \tag{27}$$

where $f_B(x) = 1/(e^x/T - 1)$ is the Bose distribution function and $\partial\omega_{\text{ph}}/\partial\phi_0$ is given from Eq. (23) by

$$\frac{\partial\omega_{\text{ph}}}{\partial\phi_0} = \epsilon \frac{3\varepsilon_{\mathbf{p}} + 2\epsilon\phi_0}{4\omega_{\text{ph}}}. \quad (28)$$

There are two limiting cases where the integration over \mathbf{p} in Eq. (27) can be analytically performed. Since the integral is dominated by the integration region where $\varepsilon_{\mathbf{p}} \sim T$, we can approximate the phonon spectrum by its linear branch $\omega_{\text{ph}}(\mathbf{p}) \simeq c_s|\mathbf{p}|$ when the temperature is very low $T \ll \epsilon\phi_0$. In this case, the integration over \mathbf{p} in Eq. (27) leads to

$$\frac{\partial V_T(\phi_0)}{\partial\phi_0} \simeq \frac{8\zeta(3)T}{\phi_0} \left(\frac{mT}{2\pi} \right)^2. \quad (29)$$

On the other hand, when the temperature is located in the intermediate region $\epsilon\phi_0 \ll T \ll \phi_0$, the phonon spectrum can be approximated by its quadratic branch $\omega_{\text{ph}} \simeq \varepsilon_{\mathbf{p}}/2$. In this case, the integration over \mathbf{p} in Eq. (27) results in

$$\frac{\partial V_T(\phi_0)}{\partial\phi_0} \simeq \epsilon \frac{(mT)^2}{4}. \quad (30)$$

Now, from the gap equation $\partial(V_{\text{eff}}(\phi) + V_T(\phi))/\partial\phi = 0$ with $\phi \equiv \phi_0 + \phi_T$, one finds the temperature dependent correction of the condensate ϕ_T satisfies

$$\frac{\partial V_{\text{eff}}(\phi_0)^2}{\partial\phi_0^2} \phi_T + \frac{\partial V_T(\phi_0)}{\partial\phi_0} = 0, \quad (31)$$

where V_{eff} is the effective potential at zero temperature in Eq. (9). To the leading order in ϵ , ϕ_T at $T \ll \epsilon\phi_0$ is given by

$$\phi_T = -\frac{8\zeta(3)T^3}{\phi_0^2}, \quad (32)$$

while at $\epsilon\phi_0 \ll T \ll \phi_0$,

$$\phi_T = -\epsilon \frac{\pi^2 T^2}{\phi_0}. \quad (33)$$

The condensate in total is $\phi = \phi_0 + \phi_T$, which decreases as the temperature increases. Note that since $\phi_T \ll \epsilon\phi_0$, the leading part of the condensate does not change in the temperature region considered here $T \ll \phi_0$. The effective potential is given by the sum of the zero temperature and finite temperature parts; $V_{\text{eff}}(\phi_0 + \phi_T) + V_T(\phi_0 + \phi_T) \simeq V_{\text{eff}}(\phi_0) + V_T(\phi_0)$.

C. Thermodynamic functions at low temperature

The temperature dependent part of the pressure P_{ph} at the low temperature region $T \ll \phi_0$ is given from the effective potential in Eq. (26) by

$$P_{\text{ph}} = -V_T(\phi_0) = -\int \frac{d\mathbf{p}}{(2\pi)^4} T \ln \left[1 - e^{-\omega_{\text{ph}}(\mathbf{p})/T} \right]. \quad (34)$$

The phonon contributions to the fermion number density, the entropy density, and the energy density are computed from the thermodynamic relations, $N_{\text{ph}} = \partial P_{\text{ph}}/\partial\mu$, $S_{\text{ph}} = \partial P_{\text{ph}}/\partial T$, and $E_{\text{ph}} = \mu N_{\text{ph}} + TS_{\text{ph}} - P_{\text{ph}}$, respectively. Here we show analytic expressions for these thermodynamic functions in the two cases where the analytic evaluation of the \mathbf{p} integration in Eq. (34) is available.

When the temperature is very low $T \ll \epsilon\phi_0$, only the linear branch of the phonon spectrum $\omega_{\text{ph}}(\mathbf{p}) \simeq c_s|\mathbf{p}|$ is important to the thermodynamic functions. In this case, the integration over \mathbf{p} can be performed analytically to lead to

$$P_{\text{ph}} \simeq \frac{12\pi^2\zeta(5)}{(2\pi)^4} \frac{T^5}{c_s^4} = \frac{12\zeta(5)}{\pi^2} \frac{m^2 T^5}{(\epsilon\phi_0)^2}. \quad (35)$$

Accordingly, we obtain the phonon contributions to the fermion number density, the entropy density, and the energy density;

$$N_{\text{ph}} = -\frac{48\zeta(5)}{\pi^2} \frac{m^2 T^5}{(\epsilon\phi_0)^3}, \quad (36)$$

$$S_{\text{ph}} = \frac{60\zeta(5)}{\pi^2} \frac{m^2 T^4}{(\epsilon\phi_0)^2}, \quad (37)$$

$$E_{\text{ph}} = \frac{24\zeta(5)}{\pi^2} \frac{m^2 T^5}{(\epsilon\phi_0)^2} \left(1 + \frac{\varepsilon_b}{\epsilon\phi_0} \right). \quad (38)$$

Since actual experiments or simulations are performed with the fixed fermion density, it is useful to show the thermodynamic functions at fixed N instead of fixed μ . From Eqs. (10), (12), and (36), we find the chemical potential for the fixed fermion density increases as a function of the temperature as

$$\mu = \mu_0 + 48\zeta(5) \frac{T^5}{\epsilon\phi_0^4}, \quad (39)$$

where μ_0 represents the chemical potential at zero temperature in Eq. (15). Normalizing μ by the Fermi energy (13), we have

$$\frac{\mu}{\varepsilon_F} = \frac{\mu_0}{\varepsilon_F} + \frac{3\zeta(5)}{2\epsilon^3} \left(\frac{2T}{\varepsilon_F} \right)^5. \quad (40)$$

The other thermodynamic functions for the fixed fermion number density are given by

$$\frac{P}{\varepsilon_F N} = \frac{P_0}{\varepsilon_F N} + \frac{3\zeta(5)}{\epsilon^3} \left(\frac{2T}{\varepsilon_F} \right)^5, \quad (41)$$

$$\frac{E}{\varepsilon_F N} = \frac{E_0}{\varepsilon_F N} + \frac{6\zeta(5)}{\epsilon^3} \left(\frac{2T}{\varepsilon_F} \right)^5, \quad (42)$$

$$\frac{S}{N} = \frac{15\zeta(5)}{\epsilon^3} \left(\frac{2T}{\varepsilon_F} \right)^4. \quad (43)$$

These expressions are valid in the low temperature region where $T \ll \epsilon\phi_0$.

On the other hand, when the temperature is located in the intermediate region $\epsilon\phi_0 \ll T \ll \phi_0$, we can expand the phonon spectrum $\omega_{\text{ph}}(\mathbf{p})$ in terms of $\epsilon\phi_0/\epsilon_p$ up to its first order

$$\omega_{\text{ph}}(\mathbf{p}) \simeq \frac{\epsilon_p}{2} + \frac{\epsilon\phi_0}{2}. \quad (44)$$

In this case, the integration over \mathbf{p} can be performed analytically again to result in

$$P_{\text{ph}} \simeq \frac{\zeta(3)}{\pi^2} m^2 T^3 - \frac{m^2 T^2}{12} \epsilon\phi_0. \quad (45)$$

Accordingly, we obtain the temperature dependent parts of the fermion number density, the entropy density, and the energy density;

$$N_{\text{ph}} = -\frac{m^2 T^2}{6}, \quad (46)$$

$$S_{\text{ph}} = \frac{3\zeta(3)}{\pi^2} m^2 T^2 - \frac{m^2 T}{6} \epsilon\phi_0, \quad (47)$$

$$E_{\text{ph}} = \frac{2\zeta(3)}{\pi^2} m^2 T^3 - \frac{m^2 T^2}{6} \epsilon\phi_0 \left(1 - \frac{\epsilon_b}{2\epsilon\phi_0}\right). \quad (48)$$

From Eqs. (10), (12), and (46), we find the chemical potential for the fixed fermion density increases as a function of the temperature as

$$\mu = \mu_0 + \epsilon^2 \frac{\pi^2}{6} \frac{T^2}{\phi_0}. \quad (49)$$

Normalizing μ by the Fermi energy in Eq. (13), we have

$$\frac{\mu}{\epsilon_F} = \frac{\mu_0}{\epsilon_F} + \epsilon^{3/2} \frac{\pi^2}{6} \left(\frac{T}{\epsilon_F}\right)^2. \quad (50)$$

The other thermodynamic functions for the fixed fermion number density are given by

$$\frac{P}{\epsilon_F N} = \frac{P_0}{\epsilon_F N} + 4\zeta(3) \left(\frac{T}{\epsilon_F}\right)^3 - \epsilon^{3/2} \frac{\pi^2}{6} \left(\frac{T}{\epsilon_F}\right)^2, \quad (51)$$

$$\frac{E}{\epsilon_F N} = \frac{E_0}{\epsilon_F N} + 8\zeta(3) \left(\frac{T}{\epsilon_F}\right)^3 - \epsilon^{3/2} \frac{\pi^2}{3} \left(\frac{T}{\epsilon_F}\right)^2, \quad (52)$$

$$\frac{S}{N} = 12\zeta(3) \left(\frac{T}{\epsilon_F}\right)^2 - \epsilon^{3/2} \frac{2\pi^2}{3} \frac{T}{\epsilon_F}. \quad (53)$$

These expressions are valid in the intermediate temperature region where $\epsilon\phi_0 \ll T \ll \phi_0$.

D. Effective potential near T_c

At the end of this section, we study the behavior of the condensate ϕ as a function of the temperature for a given μ . The effective potential to the leading order in ϵ is given by one-loop diagrams of fermion with and

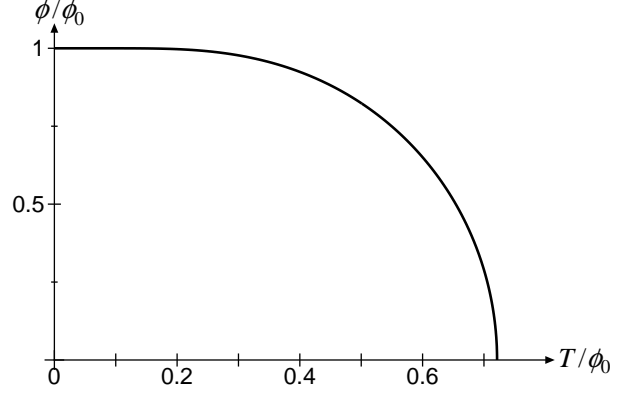


FIG. 4: The behavior of the condensate ϕ as a function of the temperature T to the lowest order in ϵ . $\phi_0 = \mu_B/\epsilon$ is the value of the condensate at $T = 0$ and the critical temperature is located at $T_c/\phi_0 = 1/(2 \ln 2) \approx 0.721348$.

without one μ insertion, which is equivalent to the mean-field approximation. Since the critical dimension of the superfluid-normal phase transition is four, the mean-field approximation remains as a leading part at any temperature in the limit $d \rightarrow 4$. Then the leading contribution to the effective potential at finite temperature is given by

$$V_{\text{eff}}(\phi) = -\frac{\epsilon_b}{g^2} \phi^2 - \int \frac{d\mathbf{p}}{(2\pi)^d} \left[E_{\mathbf{p}} - \frac{\epsilon_{\mathbf{p}}}{E_{\mathbf{p}}} \mu + 2T \ln \left(1 + e^{-E_{\mathbf{p}}/T}\right) + f_F(E_{\mathbf{p}}) \frac{2\epsilon_{\mathbf{p}}}{E_{\mathbf{p}}} \mu\right], \quad (54)$$

where $f_F(x) = 1/(e^{x/T} + 1)$ is the Fermi distribution function.

For the low temperature $T \ll \phi$, we can neglect the exponentially small factor $e^{-E_{\mathbf{p}}/T} \ll 1$ and the integration over \mathbf{p} reproduces the effective potential at zero temperature in Eq. (9). In the opposite limit where $\phi \ll T$, we can expand V_{eff} in terms of ϕ/T to lead to

$$\begin{aligned} V_{\text{eff}}(\phi) - V_{\text{eff}}(0) &= \left[T \ln 2 - \frac{\mu_B}{2\epsilon}\right] \left(\frac{m\phi}{2\pi}\right)^2 + \frac{\phi^2}{16T} \left(\frac{m\phi}{2\pi}\right)^2 + \dots, \end{aligned} \quad (55)$$

where $\mu_B = 2\mu + \epsilon_b$. From the coefficient of the quadratic term in ϕ , we can read the critical temperature T_c to the leading order in ϵ as

$$T_c = \frac{\mu_B}{\epsilon 2 \ln 2}. \quad (56)$$

The value of the condensate ϕ in the intermediate range of the temperature is obtained by solving the gap equation $\partial V_{\text{eff}}/\partial\phi = 0$;

$$\phi - \frac{\mu_B}{\epsilon} + \int d\mathbf{p} \frac{2\epsilon_{\mathbf{p}}}{E_{\mathbf{p}}} f_F(E_{\mathbf{p}}) = 0. \quad (57)$$

The numerical solution of the gap equation as a function of T is shown in Fig. 4.

IV. THERMODYNAMICS ABOVE T_c

A. Power counting rule of ϵ near T_c

In the ϵ expansion at the zero or low temperature region, the chemical potential is small compared to the condensate $\mu \sim \epsilon \phi_0$ and we made expansions in terms of $\mu/\phi_0 \sim \epsilon$ as well as the small coupling $g \sim \epsilon^{1/2}$. Near the critical temperature, the ratio μ/ϕ is no longer small because ϕ vanishes at $T = T_c$, but μ/T_c is $O(\epsilon)$ as it is clear from $T_c = \mu_B/(\epsilon 2 \ln 2)$. Therefore, we can still treat the chemical potential as a small perturbation near T_c and the same power counting rule of ϵ described in Sec. II B holds even above T_c just by replacing ϕ_0 with T . Hereafter we consider $T \sim T_c$ to be $O(1)$.

B. Boson's thermal mass

First we study the self-energy of boson at $T \geq T_c$. The leading contribution to the self-energy is the chemical potential insertion μ_B as well as the one-loop diagram Π_{11} shown in Fig. 2:

$$\begin{aligned} \Pi_{11}(i\nu, \mathbf{p}) - \Pi_0(i\nu, \mathbf{p}) &= g^2 T \sum_n \int \frac{d\mathbf{k}}{(2\pi)^d} G_{11}(i\omega_n + i\nu, \mathbf{k} + \mathbf{p}) G_{22}(i\omega_n, \mathbf{k}) \\ &= -g^2 \int \frac{d\mathbf{k}}{(2\pi)^d} \frac{1 - f_F(\varepsilon_{\mathbf{k}-\mathbf{p}/2}) - f_F(\varepsilon_{\mathbf{k}+\mathbf{p}/2})}{2\varepsilon_{\mathbf{k}} - i\nu + \varepsilon_{\mathbf{p}}/2}. \end{aligned} \quad (58)$$

C. Pressure

Now we calculate the thermodynamic functions at $T \geq T_c$ to the leading and next-to-leading orders in ϵ . There are three types of diagrams contributing to the pressure up to the next-to-leading order in ϵ as depicted in Fig. 5; one-loop diagrams with and without one μ (μ_B) insertion and two-loop diagram with a boson exchange. Note that at $T \geq T_c$, the boson's one-loop diagram contributes as $O(1)$ as well as the fermion's one-loop diagram. Then the pressure from the one-loop diagrams is given by

$$\begin{aligned} P_1 &= \int \frac{d\mathbf{p}}{(2\pi)^d} \left[2T \ln \left(1 + e^{-\varepsilon_{\mathbf{p}}/T} \right) - T \ln \left(1 - e^{-\varepsilon_{\mathbf{p}}/2T} \right) + 2\mu f_F(\varepsilon_{\mathbf{p}}) + \mu_B f_B(\varepsilon_{\mathbf{p}}/2) \right] \\ &= T \left[\frac{11}{2} \zeta(3) - \frac{9 \ln 2 \zeta(3) + 11 \zeta'(3)}{4} \epsilon + \frac{\pi^2}{6} \frac{\mu}{T} + \frac{2\pi^2}{3} \frac{\mu_B}{T} \right] \left(\frac{mT}{2\pi} \right)^{d/2}. \end{aligned} \quad (60)$$

The contribution from the two-loop diagram to the pressure, which is $O(\epsilon)$, is given by

$$\begin{aligned} P_2 &= g^2 T^2 \sum_{n,m} \int \frac{d\mathbf{p} d\mathbf{q}}{(2\pi)^{2d}} G_{11}(i\omega_n, \mathbf{p}) G_{22}(i\omega_m, \mathbf{q}) D(i\omega_n - i\omega_m, \mathbf{p} - \mathbf{q}) \\ &= -g^2 \int \frac{d\mathbf{p} d\mathbf{q}}{(2\pi)^{2d}} \frac{f_F(\varepsilon_{\mathbf{p}}) f_F(\varepsilon_{\mathbf{q}}) + [f_F(\varepsilon_{\mathbf{p}}) + f_F(\varepsilon_{\mathbf{q}})] f_B(\varepsilon_{\mathbf{p}-\mathbf{q}/2})}{\varepsilon_{\mathbf{p}} + \varepsilon_{\mathbf{q}} - \varepsilon_{\mathbf{p}-\mathbf{q}}/2}. \end{aligned} \quad (61)$$

The numerical integrations over \mathbf{p} and \mathbf{q} result in

$$P_2 = -C_P \epsilon \left(\frac{mT}{2\pi} \right)^{d/2} T, \quad (62)$$

For the zero Matsubara frequency mode $\nu_n = 0$ at the small momentum $\varepsilon_{\mathbf{p}} \ll T$, we have

$$\Pi_{11}(0, \mathbf{0}) \simeq g^2 \int \frac{d\mathbf{k}}{(2\pi)^4} \frac{f_F(\varepsilon_{\mathbf{k}})}{\varepsilon_{\mathbf{k}}} = \epsilon T 2 \ln 2. \quad (59)$$

Therefore, the zero Matsubara frequency mode has the non-negative thermal mass $\Pi_T = \epsilon T 2 \ln 2 - \mu_B \sim \epsilon$ at $T \geq T_c$. The condition of the vanishing thermal mass $\Pi_T = 0$ gives the critical temperature $T_c = \mu_B/(\epsilon 2 \ln 2)$ equivalent to Eq. (56). As we will see below, at a sufficiently high order in the perturbation theory near T_c [ϵ^2 (ϵ) compared to the leading term in the pressure (fermion density)], the resummation of the boson self-energy is needed to avoid infrared singularities appearing in the zero Matsubara frequency mode.

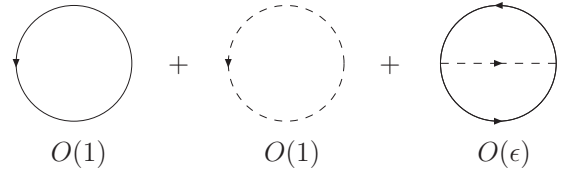


FIG. 5: Three types of diagrams contributing to the pressure up to the next-to-leading order in ϵ . Each μ (μ_B) insertion to the fermion (boson) line reduces the power of ϵ by one.

where $C_P \approx 8.4144$. From Eqs. (60) and (62), we obtain the pressure up to the next-to-leading order in ϵ as

$$P = P_1 + P_2 = T \left[\frac{11}{2} \zeta(3) - \frac{9 \ln 2 \zeta(3) + 11 \zeta'(3)}{4} \epsilon - \epsilon C_P + \frac{\pi^2}{6} \frac{\mu}{T} + \frac{2\pi^2}{3} \frac{\mu_B}{T} \right] \left(\frac{mT}{2\pi} \right)^{d/2}. \quad (63)$$

The entropy density S and the energy density E to the same order can be computed from the thermodynamic relations $S = \partial P / \partial T$ and $E = \mu N + TS - P$.

D. Fermion number density

The fermion number density to the next-to-leading order in ϵ can not be obtained simply by differentiating the pressure in Eq. (63) with respect to the chemical potential $N = \partial P / \partial \mu$. Since the pressure to the leading order in ϵ does not depend on μ and the μ derivative $\partial / \partial \mu \sim 1/\epsilon$ enhances the power of ϵ by one, we need to compute the one-loop diagrams with two μ (μ_B) insertions and two-loop diagrams with one μ (μ_B) insertion. Then the fermion density from the fermion's one-loop diagrams is given by

$$\begin{aligned} N_F &= 2 \int \frac{d\mathbf{p}}{(2\pi)^d} \left[f_F(\varepsilon_{\mathbf{p}}) + \frac{\mu}{T} f_F(\varepsilon_{\mathbf{p}}) f_F(-\varepsilon_{\mathbf{p}}) \right] \\ &= \left[\frac{\pi^2}{6} - \frac{\pi^2 \ln 2 + 6 \zeta'(2)}{12} \epsilon + \frac{2 \ln 2}{T} \mu \right] \left(\frac{mT}{2\pi} \right)^{d/2}. \end{aligned} \quad (64)$$

On the other hand, the boson's one-loop diagrams contribute to the fermion density as

$$N_B = 2 \int \frac{d\mathbf{p}}{(2\pi)^d} \left[f_B(\varepsilon_{\mathbf{p}}/2) - \frac{\mu_B}{T} f_B(\varepsilon_{\mathbf{p}}/2) f_B(-\varepsilon_{\mathbf{p}}/2) \right]. \quad (65)$$

Apparently, the last term has an infrared singularity because the Bose distribution function behaves as $f_B(\varepsilon_{\mathbf{p}}/2) \simeq 2T/\varepsilon_{\mathbf{p}}$ at the small momentum $\varepsilon_{\mathbf{p}} \ll T$. In order to resolve this infrared singularity, the resummation of the boson self-energy $\Pi_{11} = \epsilon T 2 \ln 2$ is needed at the small momentum region $\varepsilon_{\mathbf{p}} \sim \mu$. Within the accuracy we are working, we can rewrite N_B as

$$N_B = 2 \int \frac{d\mathbf{p}}{(2\pi)^d} \left[f_B(\varepsilon_{\mathbf{p}}/2 + \Pi_T) - \epsilon 2 \ln 2 f_B(\varepsilon_{\mathbf{p}}/2) f_B(-\varepsilon_{\mathbf{p}}/2) \right], \quad (66)$$

where $\Pi_T = \epsilon T 2 \ln 2 - \mu_B$. Now the first term is infrared finite, where the boson's thermal mass $\Pi_T/T = (2 \ln 2) \epsilon - \mu_B/T$ plays a role of an infrared cutoff. Integrating over \mathbf{p} and expanding up to the next-to-leading order in ϵ , we have

$$2 \int \frac{d\mathbf{p}}{(2\pi)^d} f_B(\varepsilon_{\mathbf{p}}/2 + \Pi_T) = \left[\frac{4\pi^2}{3} - \frac{2\pi^2 \ln 2 + 12 \zeta'(2)}{3} \epsilon - 8 \left(1 - \ln \frac{\Pi_T}{T} \right) \frac{\Pi_T}{T} + O(\epsilon^2) \right] \left(\frac{mT}{2\pi} \right)^{d/2}. \quad (67)$$

The logarithmic term $\sim \ln \Pi_T/T$ appears as a consequence of the resummation. The second term in Eq. (66), which is still infrared divergent, will cancel with the infrared singularity existing in the two-loop diagram.

The contribution from the two-loop diagrams to the fermion density is given by

$$N_2 = -g^2 \int \frac{d\mathbf{k} d\mathbf{p}}{(2\pi)^{2d}} \frac{f_F(\varepsilon_{\mathbf{k}+\mathbf{p}}/2) f_F(-\varepsilon_{\mathbf{k}+\mathbf{p}}/2) [f_F(\varepsilon_{\mathbf{k}-\mathbf{p}}/2) + f_B(\varepsilon_{\mathbf{p}}/2)] - 2 f_F(\varepsilon_{\mathbf{k}+\mathbf{p}}/2) f_B(\varepsilon_{\mathbf{p}}/2) f_B(-\varepsilon_{\mathbf{p}}/2)}{\varepsilon_{\mathbf{k}} T}. \quad (68)$$

The second term in the numerator contains the infrared singularity at small $\varepsilon_{\mathbf{p}}$. Extracting the divergent part, we can rewrite N_2 as

$$\begin{aligned} N_2 &= -g^2 \int \frac{d\mathbf{k} d\mathbf{p}}{(2\pi)^{2d}} \frac{f_F(\varepsilon_{\mathbf{k}+\mathbf{p}}/2) f_F(-\varepsilon_{\mathbf{k}+\mathbf{p}}/2) [f_F(\varepsilon_{\mathbf{k}-\mathbf{p}}/2) + f_B(\varepsilon_{\mathbf{p}}/2)] - 2 [f_F(\varepsilon_{\mathbf{k}+\mathbf{p}}/2) - f_F(\varepsilon_{\mathbf{k}})] f_B(\varepsilon_{\mathbf{p}}/2) f_B(-\varepsilon_{\mathbf{p}}/2)}{\varepsilon_{\mathbf{k}} T} \\ &\quad + 2g^2 \int \frac{d\mathbf{k} d\mathbf{p}}{(2\pi)^{2d}} \frac{f_F(\varepsilon_{\mathbf{k}})}{\varepsilon_{\mathbf{k}} T} f_B(\varepsilon_{\mathbf{p}}/2) f_B(-\varepsilon_{\mathbf{p}}/2). \end{aligned} \quad (69)$$

One finds the \mathbf{k} integration in the second term can be performed to lead to $\Pi_{11} = \epsilon T 2 \ln 2$ in Eq. (59), which exactly cancels out the infrared divergent part in Eq. (66). The numerical integrations over \mathbf{k} and \mathbf{p} in the first term result in

$$N_2 = -C_N \epsilon \left(\frac{mT}{2\pi} \right)^{d/2} + \epsilon 4 \ln 2 \int \frac{d\mathbf{p}}{(2\pi)^d} f_B(\varepsilon_{\mathbf{p}}/2) f_B(-\varepsilon_{\mathbf{p}}/2), \quad (70)$$

where $C_N \approx 1.92181$. Gathering up all contributions, Eqs. (64), (66), and (70), the fermion number density to the leading and next-to-leading orders is given by

$$\begin{aligned} N &= N_F + N_B + N_2 \\ &= \left[\frac{3\pi^2}{2} - \frac{3\pi^2 \ln 2 + 18\zeta'(2)}{4} \epsilon - \epsilon C_N + \frac{2 \ln 2}{T} \mu - 8 \left(1 - \ln \frac{\Pi_T}{T} \right) \frac{\Pi_T}{T} \right] \left(\frac{mT}{2\pi} \right)^{d/2}. \end{aligned} \quad (71)$$

We define the Fermi energy ε_F through the relationship in Eq. (13) as

$$\frac{\varepsilon_F}{T} = \sqrt{\frac{3\pi^2}{2}} \left[1 + \left\{ \frac{2\gamma - 3 - 2\ln 2}{8} - \frac{3\zeta'(2)}{2\pi^2} - \frac{C_N}{3\pi^2} + \frac{1}{8} \ln \left(\frac{3\pi^2}{2} \right) \right\} \epsilon + \frac{2\ln 2}{3\pi^2} \frac{\mu}{T} - \frac{8}{3\pi^2} \left(1 - \ln \frac{\Pi_T}{T} \right) \frac{\Pi_T}{T} \right]. \quad (72)$$

The logarithmic correction $(\Pi_T/T) \ln \Pi_T/T \sim \epsilon \ln \epsilon$ is a consequence of the resummation to avoid the infrared singularities, while it vanishes at the critical temperature $\Pi_{T_c} = \epsilon T_c 2 \ln 2 - \mu_B = 0$.

E. Critical temperature

The critical temperature in units of the Fermi energy directly follows from Eq. (72) with the use of the relationship $2\mu + \varepsilon_b = \epsilon T_c 2 \ln 2$:

$$\begin{aligned} \frac{T_c}{\varepsilon_F} &= \sqrt{\frac{2}{3\pi^2}} \left[1 - \left\{ \frac{2\gamma - 3 - 2\ln 2}{8} - \frac{3\zeta'(2)}{2\pi^2} \right. \right. \\ &\quad \left. \left. - \frac{C_N - 2(\ln 2)^2}{3\pi^2} + \frac{1}{8} \ln \left(\frac{3\pi^2}{2} \right) \right\} \epsilon \right] + \frac{\ln 2}{3\pi^2} \frac{\varepsilon_b}{\varepsilon_F} \\ &= 0.260 - 0.0112 \epsilon + 0.0234 \frac{\varepsilon_b}{\varepsilon_F} + O(\epsilon^2), \end{aligned} \quad (73)$$

where the numerical value $C_N \approx 1.92181$ is substituted. We find the critical temperature T_c is an increasing function of the binding energy ε_b near the unitarity limit. The next-to-leading order correction is reasonably small compared to the leading term even at $\epsilon = 1$. The naive extrapolation of the critical temperature to the physical case of $d = 3$ gives $T_c/\varepsilon_F \approx 0.249$ in the unitarity limit $\varepsilon_b = 0$. This value is surprisingly close to results from some Monte Carlo simulations, $T_c/\varepsilon_F = 0.23(2)$ [32] and $T_c/\varepsilon_F \approx 0.25$ [35], while others provide smaller values, $T_c/\varepsilon_F < 0.14$ [33] and $T_c/\varepsilon_F = 0.152(7)$ [34].

The more appropriate estimate of T_c at $d = 3$ will be obtained by matching the ϵ expansion with the exact result around $d = 2$. The critical temperature at unitarity in the expansion over $\bar{\epsilon} = d - 2$ is given by $T_c = (e^\gamma/\pi) \Delta$, where $\Delta/\varepsilon_F = (2/e) e^{-1/\bar{\epsilon}}$ is the energy gap of the fermion quasiparticle at zero temperature [14]:

$$\frac{T_c}{\varepsilon_F} = \frac{2e^{\gamma-1}}{\pi} e^{-1/\bar{\epsilon}} [1 + O(\bar{\epsilon})]. \quad (74)$$

We shall write the power series of $\bar{\epsilon}$ in the form of the Borel transformation,

$$\frac{T_c(\bar{\epsilon})}{\varepsilon_F} = \frac{2e^{\gamma-1}}{\pi} e^{-1/\bar{\epsilon}} \int_0^\infty dt e^{-t} B_{T_c}(\bar{\epsilon}t). \quad (75)$$

$B_{T_c}(t)$ is the Borel transform of the power series in $T_c(\bar{\epsilon})$, whose Taylor coefficients at origin is given by

$B_{T_c}(t) = 1 + \dots$. In order to perform the integration over t in Eq. (75), the analytic continuation of the Borel transform $B_{T_c}(t)$ to the real positive axis of t is necessary. Here we employ the Padé approximation, where $B_{T_c}(t)$ is approximated by the following rational functions

$$B_{T_c}(t) = \frac{1 + p_1 t + \dots + p_M t^M}{1 + q_1 t + \dots + q_N t^N}. \quad (76)$$

Then we incorporate the results around four spatial dimensions in Eq. (73) by imposing

$$\frac{T_c(2 - \epsilon)}{\varepsilon_F} = 0.260 - 0.0112 \epsilon + \dots \quad (77)$$

on the Padé approximants as a boundary condition. Since we have two known coefficients from the ϵ expansion, the Padé approximants $[M/N]$ satisfying $M+N=2$ are possible. Since we could not find a solution satisfying the boundary condition in Eq. (77) for $[M/N] = [1/1]$, we adopt other two Padé approximants with $[M/N] = [2/0], [0/2]$, whose coefficients p_m and q_n are determined uniquely by the above conditions.

Fig. 6 shows the critical temperature T_c in units of the Fermi energy ε_F as a function of the spatial dimensions d . The middle two curves show T_c/ε_F in the different Padé approximants connecting the two expansions around $d = 4$ and $d = 2$. These Borel-Padé approximations give $T_c/\varepsilon_F = 0.173$ and 0.192 at $d = 3$, which are located between the naive extrapolations to $d = 3$ from the $\epsilon = 4 - d$ expansion ($T_c/\varepsilon_F \rightarrow 0.249$) and the $\bar{\epsilon} = d - 2$ expansion ($T_c/\varepsilon_F \rightarrow 0.153$). It is also interesting to compare our results with those from the recent Monte Carlo simulations, where $T_c/\varepsilon_F = 0.23(2)$ [32], $T_c/\varepsilon_F < 0.14$ [33], $T_c/\varepsilon_F = 0.152(7)$ [34], and $T_c/\varepsilon_F \approx 0.25$ [35]. Although these results from the Monte Carlo simulations seem not to be settled, the interpolation of the two expansions provides the moderate value $T_c/\varepsilon_F = 0.183 \pm 0.014$ not too far from the Monte Carlo simulations.

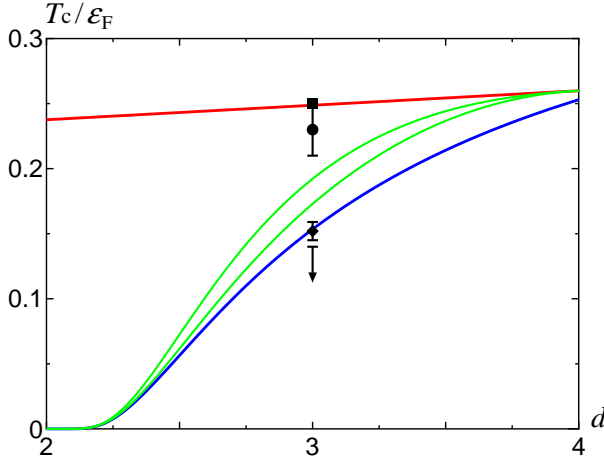


FIG. 6: The critical temperature T_c at unitarity as a function of the spatial dimensions d . The upper solid line is from the expansion around $d = 4$ in Eq. (73), while the lower solid line is from the expansion around $d = 2$ in Eq. (74). The middle two curves show the different Borel–Padé approximations connecting the two expansions. The symbols at $d = 3$ indicate the results from the Monte Carlo simulations; $T_c/\varepsilon_F = 0.23(2)$ [32] (circle), $T_c/\varepsilon_F < 0.14$ [33] (down arrow), $T_c/\varepsilon_F = 0.152(7)$ [34] (diamond), and $T_c/\varepsilon_F \approx 0.25$ [35] (square).

F. Thermodynamic functions at T_c

Finally we show the thermodynamic functions at T_c in the unitarity limit $\varepsilon_b = 0$ to the leading and next-to-leading orders in ϵ . The pressure P normalized by the fermion density $\varepsilon_F N$ follows from Eqs. (63), (71), and (72). Introducing the numerical values $C_P \approx 8.4144$ and $C_N \approx 1.92181$, we obtain the pressure up to the next-to-leading order in ϵ as

$$\frac{P}{\varepsilon_F N} \Big|_{T_c} = 0.116 + 0.0188 \epsilon. \quad (78)$$

From the universal relationship in the unitarity limit $E = (d/2)P$, the energy density is given by

$$\frac{E}{\varepsilon_F N} \Big|_{T_c} = 0.232 - 0.0205 \epsilon. \quad (79)$$

The chemical potential at the critical temperature $\mu = \epsilon T_c \ln 2$ is $O(\epsilon)$. Normalizing μ by the Fermi energy in Eq. (73), we have

$$\frac{\mu}{\varepsilon_F} \Big|_{T_c} = \epsilon \ln 2 \sqrt{\frac{2}{3\pi^2}} = 0.180 \epsilon. \quad (80)$$

Then the entropy density $T_c S = (d/2+1)P - \mu N$ is given by

$$\frac{S}{N} \Big|_{T_c} = 1.340 - 0.642 \epsilon. \quad (81)$$

The next-to-leading order corrections to the pressure and energy density are reasonably small compared to the leading order terms, while that is large for the entropy density.

We match the thermodynamic functions at T_c in the expansions over $\epsilon = 4 - d$ with those around $d = 2$ as we demonstrated for T_c/ε_F . The critical temperature around $d = 2$ is $T_c/\varepsilon_F \sim e^{-1/\bar{\epsilon}}$, which is exponentially small and negligible compared to any power series of $\bar{\epsilon}$. Therefore, the pressure, energy density, and chemical potential at T_c in the expansions over $\bar{\epsilon} = d - 2$ is simply given by those at zero temperature [14];

$$\frac{P}{\varepsilon_F N} \Big|_{T_c} = \frac{2}{d+2} \xi = \frac{1}{2} - \frac{5}{8} \bar{\epsilon}, \quad (82)$$

$$\frac{E}{\varepsilon_F N} \Big|_{T_c} = \frac{d}{d+2} \xi = \frac{1}{2} - \frac{3}{8} \bar{\epsilon}, \quad (83)$$

$$\frac{\mu}{\varepsilon_F} \Big|_{T_c} = \xi = 1 - \bar{\epsilon}. \quad (84)$$

A straightforward calculation shows that the entropy per particle at T_c to the leading order in $\bar{\epsilon}$ is given by

$$\frac{S}{N} \Big|_{T_c} = \frac{\pi^2}{3} \frac{T_c}{\varepsilon_F} = \frac{2\pi e^{\gamma-1}}{3} e^{-1/\bar{\epsilon}}. \quad (85)$$

Using the Borel–Padé approximations connecting the two expansions above, thermodynamic functions at $d = 3$ are found to be $P/(\varepsilon_F N)|_{T_c} = 0.172 \pm 0.022$, $E/(\varepsilon_F N)|_{T_c} = 0.270 \pm 0.004$, $\mu/\varepsilon_F|_{T_c} = 0.294 \pm 0.013$, and $S/N|_{T_c} = 0.642$. The errors here indicates only the uncertainty due to the choice of different Padé approximants. In the recent Monte Carlo simulation, the thermodynamic functions at the critical temperature is $P/(\varepsilon_F N)|_{T_c} = 0.207(7)$, $E/(\varepsilon_F N)|_{T_c} = 0.31(1)$, $\mu/\varepsilon_F|_{T_c} = 0.493(14)$, and $S/N|_{T_c} = 0.16(2)$ [34]. We see that the interpolations of the two expansions indeed improve the series summations compared to the naive extrapolations from $d = 4$ or $d = 2$, while there still exist deviations between our results and the Monte Carlo simulation. We can understand these deviations partially due to the difference in the determined critical temperature. The large deviations existing in μ/ε_F and S/N may be because we know only the leading term for μ and the next-to-leading order correction for S is sizable.

V. SUMMARY AND CONCLUDING REMARKS

In this paper, the thermodynamics of the Fermi gas near the unitarity limit at finite temperature has been investigated using the systematic expansion over $\epsilon = 4 - d$. We discussed that the thermodynamics in the low temperature region $T \ll T_c$ is dominated by the bosonic phonon excitations. The analytic formulas for the thermodynamic functions at the fixed fermion density are de-

rived in the two limiting cases; $T \ll \epsilon T_c$ in Eqs. (40)–(43) and $\epsilon T_c \ll T \ll T_c$ in Eqs. (50)–(53).

In the high temperature region $T \sim T_c$, the fermionic quasiparticles are excited as well as the bosonic quasiparticles. We showed that the similar power counting rule of ϵ to that developed at zero temperature works even above T_c . The critical temperature T_c and the thermodynamic functions around T_c were calculated to the leading and next-to-leading orders in ϵ . We found the critical temperature is an increasing function of the binding energy ϵ_b near the unitarity limit:

$$\frac{T_c}{\epsilon_F} = 0.260 - 0.0112\epsilon + 0.0234\frac{\epsilon_b}{\epsilon_F}. \quad (86)$$

The next-to-leading order correction is reasonably small compared to the leading term even at $\epsilon = 1$. In the unitarity limit $\epsilon_b = 0$, the naive extrapolation of the critical temperature to the physical case of $d = 3$ gives $T_c/\epsilon_F \approx 0.249$.

We also discussed the matching of the ϵ expansion with the expansion around $d = 2$. The critical temperature at unitarity in the expansion over $\bar{\epsilon} = d - 2$ is given by $T_c/\epsilon_F = (2e^{\gamma-1}/\pi)e^{-1/\bar{\epsilon}}$, where its naive extrapolation to $\bar{\epsilon} = 1$ gives $T_c/\epsilon_F \approx 0.153$. The Borel–Padé approximations connecting the two expansions yielded $T_c/\epsilon_F = 0.183 \pm 0.014$ at $d = 3$, which is a moderate value located between the two naive extrapolations [Fig. 6]. These values are not too far from the results obtained

by the recent Monte Carlo simulations where $T_c/\epsilon_F = 0.15 \sim 0.25$ [32, 34, 35]. We also applied the Borel–Padé approximations to the thermodynamic functions at T_c , which yielded $P/(\epsilon_F N)|_{T_c} \approx 0.172$, $E/(\epsilon_F N)|_{T_c} \approx 0.270$, $\mu/\epsilon_F|_{T_c} \approx 0.294$, and $S/N|_{T_c} \approx 0.642$ at $d = 3$.

The Borel–Padé approximations employed here to match the two expansions around two and four spatial dimensions do not correctly reflect the large order behavior of the expansion around $d = 2$, i.e., the Borel transform $B(t)$ of the series expansion over $\bar{\epsilon} = d - 2$ has a singularity at $t = 2$ [14]. Furthermore, an understanding of the structure of high-order terms in the perturbation theory around $d = 4$ is currently lacking. In order for the accurate determination of the critical temperature and the thermodynamic functions at $d = 3$, it will be important to appropriately take into account the knowledge on the large order behaviors of the expansions both around two and four spatial dimensions. The calculation of higher order corrections to our results is also interesting. These problems should be studied in future works.

Acknowledgments

The author would like to thank D. T. Son for useful discussions. This research was supported by the Japan Society for the Promotion of Science for Young Scientists.

[1] D. M. Eagles, Phys. Rev. **186**, 456 (1969).
[2] A. J. Leggett, in *Modern Trends in the Theory of Condensed Matter* (Springer, Berlin, 1980).
[3] P. Nozières and S. Schmitt-Rink, J. Low Temp. Phys. **59**, 195 (1985).
[4] K. M. O’Hara *et al.*, Science **298**, 2179 (2002).
[5] C. A. Regal, M. Greiner, and D. S. Jin, Phys. Rev. Lett. **92**, 040403 (2004).
[6] M. Bartenstein *et al.*, Phys. Rev. Lett. **92**, 120401 (2004).
[7] M. W. Zwierlein *et al.*, Phys. Rev. Lett. **92**, 120403 (2004).
[8] J. Kinast *et al.*, Phys. Rev. Lett. **92**, 150402 (2004).
[9] T. Bourdel *et al.*, Phys. Rev. Lett. **93**, 050401 (2004).
[10] J. Kinast *et al.*, Science **307**, 1296 (2005).
[11] G. Bertsch, *Many-Body X Challenge*, in: Proc. X Conference on Recent Progress in Many-Body Theories, eds. R. F. Bishop *et al.* (World Scientific, Singapore, 2000).
[12] See, e.g., Q. Chen, J. Stajic, S. Tan, and K. Levin, Phys. Rep. **412**, 1 (2005), and references therein.
[13] Y. Nishida and D. T. Son, Phys. Rev. Lett. **97**, 050403 (2006).
[14] Y. Nishida and D. T. Son, arXiv:cond-mat/0607835.
[15] Z. Nussinov and S. Nussinov, arXiv:cond-mat/0410597.
[16] G. Rupak, arXiv:nucl-th/0605074.
[17] G. Rupak, T. Schaefer and A. Kryjevski, arXiv:cond-mat/0607834.
[18] C. A. R. Sá de Melo, M. Randeria and J. R. Engelbrecht, Phys. Rev. Lett. **71**, 3202 (1993).
[19] R. Haussmann, Z. Phys. B **91**, 291 (1993); Phys. Rev. B **49**, 12975 (1994).
[20] M. Holland, S. J. J. M. F. Kokkelmans, M. L. Chiofalo, and R. Walser, Phys. Rev. Lett. **87**, 120406 (2001).
[21] E. Timmermans, K. Furuyab, P. W. Milonni, and A. K. Kermanc, Phys. Lett. A **285**, 228 (2001).
[22] Y. Ohashi and A. Griffin, Phys. Rev. Lett. **89**, 130402 (2002); Phys. Rev. A **67**, 033603 (2003).
[23] J. N. Milstein, S. J. J. M. F. Kokkelmans, and M. J. Holland, Phys. Rev. A **66**, 043604 (2002).
[24] A. Perali, P. Pieri, L. Pisani, and G. C. Strinati, Phys. Rev. Lett. **92**, 220404 (2004).
[25] X.-J. Liu and H. Hu, Phys. Rev. A **72**, 063613 (2005).
[26] Y. Nishida and H. Abuki, Phys. Rev. D **72**, 096004 (2005).
[27] H. Abuki, arXiv:hep-ph/0605081.
[28] T.-L. Ho and E. J. Mueller, Phys. Rev. Lett. **92**, 160404 (2004).
[29] C. J. Horowitz and A. Schwenk, Phys. Lett. B **638**, 153 (2006).
[30] G. Rupak, arXiv:nucl-th/0604053.
[31] M. Wingate, arXiv:cond-mat/0502372.
[32] A. Bulgac, J. E. Drut, and P. Magierski, Phys. Rev. Lett. **96**, 090404 (2006).
[33] D. Lee and T. Schafer, Phys. Rev. C **73**, 015201 (2006); Phys. Rev. C **73**, 015202 (2006).

[34] E. Burovski, N. Prokofev, B. Svistunov, and M. Troyer, Phys. Rev. Lett. **96**, 160402 (2006); arXiv:cond-mat/0605350.

[35] V. K. Akkineni, D. M. Ceperley, and N. Trivedi, arXiv:cond-mat/0608154.